Elsevier Editorial(tm) for Journal of Molecular Spectroscopy
Manuscript Draft

Manuscript Number:

Title: The rotationally-resolved absorption spectrum of formaldehyde from 6547 to 6804 cm-1

Article Type: Regular Article

Keywords: formaldehyde; H2CO; near infrared absorption spectrum; combination bands; cavity enhanced absorption spectroscopy; CEAS; pressure broadening; high resolution

Corresponding Author: Dr. Albert A. Ruth National University of Ireland

Other Authors: Michael Staak, Dipl. Phys.; Edward W. Gash, PhD; Dean S. Venables, PhD; NUI University College Cork, NUI University College Cork, NUI University College Cork

# The rotationally-resolved absorption spectrum of formaldehyde from 6547 to 6804 $cm^{-1}$

Michael Staak, Edward W. Gash, Dean S. Venables, Albert A. Ruth *

*Department of Physics, National University of Ireland, University College Cork, Cork, Ireland*

**Abstract**

The room temperature absorption spectrum of formaldehyde, $H_2CO$, from 6547 to 6804 $cm^{-1}$ (1527 to 1470 nm) is reported with a spectral resolution of 0.001 $cm^{-1}$. The spectrum was measured using cavity-enhanced absorption spectroscopy (CEAS) and absorption cross-sections were calculated after calibrating the system using known absorption lines of $H_2O$ and $CO_2$. Several vibrational combination bands occur in this region and give rise to a congested spectrum with over 8000 lines observed. Pressure broadening coefficients in $N_2$, $O_2$, and $H_2CO$ are reported for an absorption line at 6780.871 $cm^{-1}$, and in $N_2$ for an absorption line at 6684.053 $cm^{-1}$.

*Key words:* Formaldehyde, $H_2CO$, near infrared spectrum, combination bands, cavity enhanced absorption spectroscopy (CEAS), pressure broadening, high resolution

## 1 Introduction

Formaldehyde has a rich chemistry in the atmosphere, where it occurs as an intermediate species in the oxidation of alkanes and alkenes, nitric oxide, and dimethyl sulphoxide [1]. The photolysis of formaldehyde, $H_2CO$:

$$H_2CO + h\nu \rightarrow H + HCO$$

and the subsequent formation of the hydroperoxyl radical, $HO_2$, in the presence of oxygen:

* Corresponding author.
*Email address:* a.ruth@ucc.ie (Albert A. Ruth).

Table 1
Transition energies for the six normal vibrational modes of $H_2CO$ [12].

| Number | Symmetry | $\tilde{\nu}$ [$cm^{-1}$] | Mode |
|---|---|---|---|
| $\nu_1$ | $a_1$ | 2782.5 | $CH_2$ symmetric stretch |
| $\nu_2$ | $a_1$ | 1746.0 | CO stretch |
| $\nu_3$ | $a_1$ | 1500.2 | $CH_2$ scissor |
| $\nu_4$ | $b_1$ | 1167.3 | $CH_2$ wag |
| $\nu_5$ | $b_2$ | 2843.3 | $CH_2$ asymmetric stretch |
| $\nu_6$ | $b_2$ | 1249.1 | $CH_2$ rock |

$$HCO + O_2 \rightarrow CO + HO_2$$
$$H + O_2 \rightarrow HO_2$$

play a key role in oxidation chain reactions. The importance of these reactions has encouraged efforts to improve the spectroscopic data on $H_2CO$ and $HO_2$ for use in field studies and laboratory experiments [2–8].

Various spectroscopic methods have been employed to measure the gas-phase absorption spectrum of $H_2CO$. To increase the sensitivity of the measurement, either a multipass cell, or cavity-enhanced spectroscopic methods such as cavity ring-down spectroscopy (CRDS) and cavity enhanced absorption spectroscopy (CEAS) [9,10], have typically been used. Barry et al. reported the $2\nu_5$ overtone band (around 5676 $cm^{-1}$) using CEAS [2], and have shown that the results from CEAS closely match those from CRDS [11]. For applying absorption spectroscopy to trace measurements of $H_2CO$, the stronger fundamental vibration bands have usually been used. For instance, Fried and co-workers used a tunable diode laser spectrometer (TDLAS) system to carry out airborne measurements of $H_2CO$ using the 2831 $cm^{-1}$ absorption line [3]. They demonstrated a detection limit of 55 ppt with an integration time of 20 s. Dahnke et al. have achieved a 2 ppb sensitivity to $H_2CO$ with cavity leak-out spectroscopy at 2853 $cm^{-1}$ [8].

In this paper we report the $H_2CO$ absorption spectrum from 6547 to 6804 $cm^{-1}$. The $H_2CO$ molecule has $C_{2v}$ symmetry and six normal modes (Table 1), with several combination bands between 6500 and 6830 $cm^{-1}$ (Table 2). These transitions have been observed with a 1 $cm^{-1}$ resolution by Bouwens et al. in a jet experiment using dispersed fluorescence spectroscopy from a number of vibrational bands in the $S_1$ excited state [13]. The $H_2CO$ combination bands consist of three to five normal modes. A sensitive spectroscopic technique is therefore necessary to measure the absorption of these combination bands' rovibrational lines. In this work we used CEAS to record the $H_2CO$ spectrum.

Although the weak $H_2CO$ absorption lines from 6547 to 6804 $cm^{-1}$ are not

Table 2
Combination bands between 6500 and 6830 $cm^{-1}$ from the dispersed fluorescence spectra of Bouwens et al. [13]. Tentatively identified combination bands observed in our spectrum are indicated with asterisks.

| Combination band | Symmetry | $\tilde{\nu}$ [$cm^{-1}$] |
|---|---|---|
| $3_2 4_2 6_1$ | $b_2$ | 6508.8 |
| $1_1 3_1 4_2$ | $a_1$ | 6562.7 |
| $2_1 4_2 6_2$ | $a_1$ | 6578.8 |
| $1_2 4_1$ | $b_1$ | 6611.6 |
| $3_1 4_2 5_1$ | $b_2$ | 6635.7* |
| $2_3 3_1$ | $a_1$ | 6652.2 |
| $2_1 3_1 4_3$ | $b_1$ | 6693.4* |
| $3_1 4_1 5_1 6_1$ | $b_1$ | 6710.0 |
| $3_1 5_1 6_2$ | $b_2$ | 6759.0 |
| $2_1 3_1 4_2 6_1$ | $b_2$ | 6777.6* |
| $4_1 5_2$ | $b_1$ | 6795.1 |
| $3_3 4_2$ | $a_1$ | 6815.2 |
| $1_1 2_1 4_2$ | $b_1$ | 6825.5 |

suited for field observations of $H_2CO$, they should be useful in laboratory studies and database development. We note that recent efforts to calculate the vibrational and rotational constants of $HO_2$ from its $2\nu_1$ spectrum (between 6603 and 6686 $cm^{-1}$) have been hampered by ambiguities in the line positions, possibly arising from interfering $H_2CO$ lines [4]. Pressure broadening coefficients in $N_2$, $O_2$, and $H_2CO$ are reported for an absorption line at 6780.871 $cm^{-1}$, and in $N_2$ for an absorption line at 6684.053 $cm^{-1}$. The integrated cross-sections of these lines are also reported.

## 2 Experimental

CEAS is based on measuring the intensity of light transmitted through a high finesse optical cavity as a function of wavelength [10,14]. In comparison, in CRDS the decay time of light in an optically stable resonator is the desired parameter. For small losses per pass, the absorption coefficient, $\alpha$, of the sam-

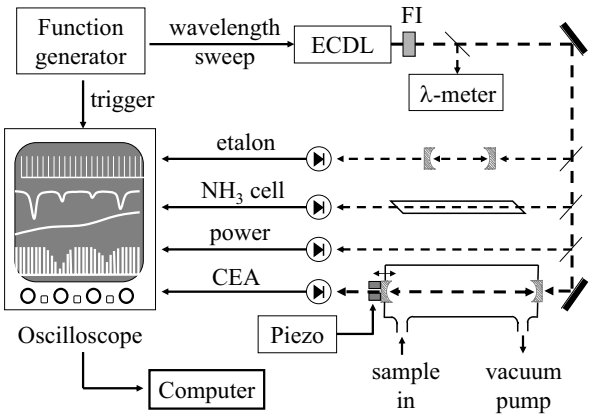


Fig. 1. Diagram of the CEAS system showing the beam path (dashed) from the external cavity diode laser (ECDL), through a Faraday isolator (FI), and through the sample cavity to give the cavity-enhanced absorption (CEA) signal. Before the sample cavity, small fractions of the beam intensity are split off to record the relative power and to calibrate the wavelength scale.

ple is adequately described by [15]:

$$\alpha \approx \frac{1}{d}\left(\frac{I_0}{I} - 1\right)(1 - R) \tag{1}$$

where $d$ is the cavity length, $R$ is the mirror reflectivity, and $I$ and $I_0$ are, respectively, the intensity transmitted through the cavity with and without a sample present. CEAS is $(1 - R)^{-1}$ times more sensitive than a single-pass absorption method assuming that the achievable signal-to-noise ratio remains the same for both approaches [16]. CEAS does not yield absorption cross-sections directly; the wavelength-dependent mirror reflectivities must be either known or calibrated against a spectrum of known absorption cross-section.

Our experimental setup is shown schematically in Fig. 1. The light source was a temperature-stabilized external cavity diode laser (Sacher Lasertechnik, TEC 500) in a Littman configuration. The laser power was ≈3 mW and the bandwidth was ∼1 MHz. The total tuning range of the system was between 6547 and 6804 $cm^{-1}$ (corresponding to 1527 and 1470 nm). The spectrum we present here covers this entire spectral range, except for two gaps near the red edge of the range (from 6549.7 to 6551.3 $cm^{-1}$ and 6553.5 to 6554.5 $cm^{-1}$) where stable laser operation was not obtained.

The laser was linearly scanned over a range of 2 $cm^{-1}$ (referred to as a "spectral segment") at approximately 40 Hz and synchronized with the oscilloscope. The laser beam was coupled into an 85 cm cavity formed by two spherical mirrors of 5 m radius of curvature and a maximum reflectivity of ∼0.996. An optical isolator was placed after the laser output aperture to reduce feedback

into the laser and associated laser instability. The distance from the laser to the cavity was also made as large as possible (2.5 m) for the same reason. The light transmitted through the cavity was detected with an InGaAs photodiode (NewFocus Nirvana 2017). For each 2 $cm^{-1}$ segment of the spectrum, 1000 sweeps were collected and averaged with a digital oscilloscope (LeCroy Waverunner LT 264). The exposure time was 10 s at a sampling rate of 4 Hz, limited by our oscilloscope. The sampling interval of 0.0008 $cm^{-1}$ was enough to resolve the $H_2CO$ Doppler-broadened FWHM of about 0.015 $cm^{-1}$.

A key consideration in CEAS is to minimize the influence of the cavity's mode structure on the wavelength-dependent intensity of the transmitted light. This is achieved by continuously modulating the cavity length in order to shift the mode structure between sweeps. A ring-shaped piezoelectric transducer attached to the cavity's exit mirror was used for this purpose. We also adopted an off-axis configuration in order to excite a large number of high order transverse modes [17]. The laser was scanned at a rapid rate of 6 MHz $\mu s^{-1}$ (0.2 $cm^{-1}s^{-1}$), which was significantly larger than the ratio of the cavity mode linewidth to the ring-down time (0.3 MHz $\mu s^{-1}$ for the $TEM_{00}$ mode). Consequently, the light intensity in a given mode was far away from saturation. These strategies avoided the build up of significant light in any single cavity mode. The transmitted intensity per frequency interval (which is determined by the integration time) is then averaged over the number of sweeps per measurement. Discrete cavity modes were not observed in the transmitted light.

Small fractions of the beam intensity were split off before the cavity to calibrate the wavenumber scale and to measure the laser power. For the wavenumber calibration, the spectrum of $NH_3$ was recorded by passing a beam through a 60 cm cell filled with $NH_3$ at 10 mbar. Absorption peaks were matched to the $NH_3$ spectrum reported by Lundsberg-Nielsen et al. [18]. The spectral density of $NH_3$ lines is high enough over the entire spectrum presented here in order to obtain several absolute wavenumbers per spectral segment. To compensate for small deviations from linearly scanning the laser over a $\sim$2 $cm^{-1}$ spectral segment, the relative wavenumber spacing was also determined from a Fabry–Perot etalon with a free-spectral range of about 0.03 $cm^{-1}$. We estimate the uncertainty in our wavenumber scale to be approximately 0.001 $cm^{-1}$ [19]. The etalon also served to identify mode-hops within the laser scanning range. When mode-hops were observed, the temperature of the laser diode was adjusted until the scanning region was mode-hop free. A third beam was used to normalize the laser power over the tuning range. These three signals were measured with InGaAs photodiodes (Thorlabs DET410) and recorded simultaneously with the cavity-enhanced absorption signal on the digital oscilloscope (see Fig 1).

$H_2CO$ was prepared by pyrolysis of paraformaldehyde (Aldrich, 95% pure) under vacuum. The gaseous $H_2CO$ was first passed through a cooling trap below

200 K to remove water vapour and polymerization products of $H_2CO$. Water vapour catalyses the polymerization of $H_2CO$. The monomeric $H_2CO$ was trapped and stored at 77 K under vacuum. The sample cavity was evacuated to approximately $10^{-6}$ mbar, ensuring that it was virtually free of gaseous water. $H_2CO$ gas was introduced into the cavity by slowly heating the solid $H_2CO$ in the cooling trap with the valve to the cavity opened. When the vapour pressure of the $H_2CO$ reached the required value of 2 mbar the valve was closed and the solid $H_2CO$ was cooled again for further use. The pressure in the cavity was measured with a capacitance manometer operating in the range of $10^{-2}$ to 120 mbar with a precision of 0.01 mbar. With 2 mbar of $H_2CO$ in the sample cavity, the pressure decreased by about 0.1 mbar before stabilizing, whereas at pressures above 10 mbar the pressure dropped by 50% over a period of a few hours. Polymerization of $H_2CO$ therefore appears to be negligible at 2 mbar. The temperature of the system was $291 \pm 2$ K.

## 3 Results and Discussion

### *3.1 Absorption spectrum*

$I_0$, $I$, and the reflectivity spectrum of the mirrors, $R$, must be known to calculate the absorption coefficient of the sample with Eq. (1). Because the measurement of $I_0$ for every corresponding 2 $cm^{-1}$ segment of the spectrum is prohibitively time-consuming for a 250 $cm^{-1}$ spectral range, we adopted a pragmatic approach to estimate $I_0$. In areas of the $H_2CO$ spectrum where no absorption occurs, the transmitted intensities with and without a sample should be the same. Therefore, an estimated $I_0$ was obtained from a fourth-order polynomial fit to well-spaced maxima in the spectrum of $I$. The absorption cross-section, $\sigma = \alpha N^{-1}$, where $N$ is the number density of the absorbing species, was calculated by using this estimated $I_0$ in Eq. (1).

The system was calibrated using the integrated cross-sections of $H_2O$ and $CO_2$ lines from the HITRAN database to calculate $R$ as a function of wavelength [20]. The corresponding calibration curves in Fig. 2 show that the integrated absorption of a transition varies linearly with the pressure, as expected. Furthermore, there is a minimal offset at the lowest pressures, suggesting that our approximation for $I_0$ does not introduce a large systematic error. From the $H_2O$ and $CO_2$ absorption lines the mirror reflectivity, $R$, was determined as a function of wavelength as shown in Fig. 3. Points with large error bars were determined from single measurements, and those with small error bars from linear regressions of pressure dependent measurements as in Fig. 2. Because the reflectivity decreases towards the blue end of the spectrum, a second-order polynomial was fitted to $(1 - R)$ as a function of wavelength. In the fit the

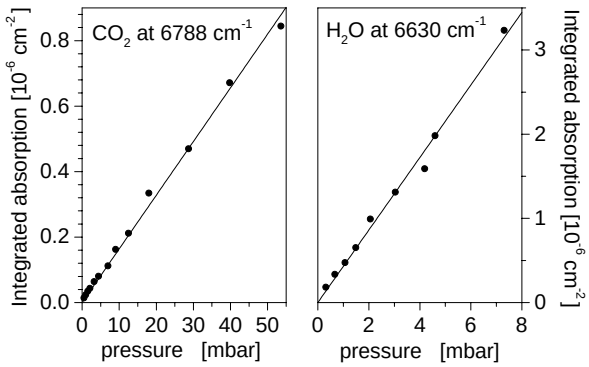


Fig. 2. Integrated absorption coefficient as a function of pressure. The left panel shows a $CO_2$ transition at 6788 $cm^{-1}$ and the right panel an $H_2O$ transition at 6630 $cm^{-1}$. The slopes of these graphs were used to calculate the mirror reflectivities at these wavenumbers.

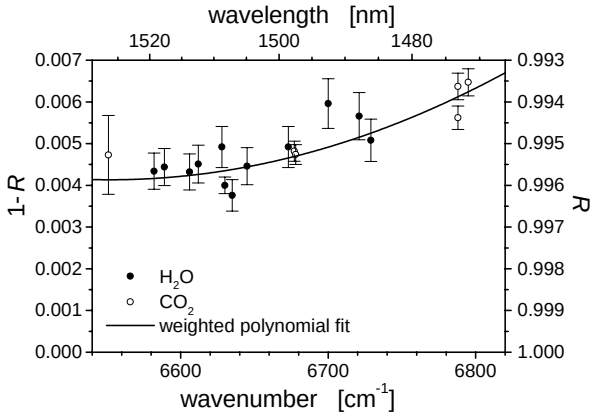


Fig. 3. Mirror reflectivity obtained using the integrated cross-sections of $H_2O$ and $CO_2$ lines from HITRAN [20]. The curve is a weighted second-order polynomial fit to the experimental points and was used for the reflectivity.

different uncertainties of calibration measurements were accounted for. The overall systematic error of this calibration of the wavelength-dependent reflectivity was established to be $\pm 5\%$. The calculated values of $R$ agree well with the manufacturer's specified maximum mirror reflectivity of 0.996 around 6500 $cm^{-1}$.

The individual segments of the spectrum were joined together to obtain the complete spectrum. The overlap of two typical spectral segments is shown in Fig. 4 and the general agreement between the absorption coefficients of such segments is very satisfactory. For the final spectrum, the overlap regions of adjacent spectral segments were averaged, or where one spectral segment was to be preferred for experimental reasons, the best measurement was chosen. The overall statistical uncertainty in the $H_2CO$ absorption cross-section is estimated at $\approx 10\%$ over most of the spectrum. However, where the laser is at its tuning limit for a given laser mode, the absorption coefficients of adjacent

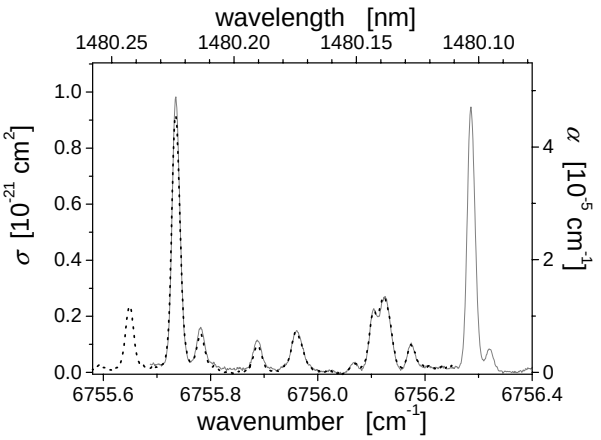


Fig. 4. Typical overlap of two adjacent spectral segments. The agreement in the wavenumber between two adjacent segments is usually within 0.001 $cm^{-1}$, and the difference in the absorption maxima is usually less than 10%.

spectral segments show poorer agreement. In these cases, which constitute less than 3% of the entire spectral range, we estimate the uncertainty in the absorption coefficients to be ≈25%. These regions are identified in the supplementary material [21]. The signal-to-noise ratio of the spectrum is better than 500. The minimum detectable absorption of our system is approximately $1.5 \times 10^{-7}$ $cm^{-1}$ with a 10 s exposure time.

Table 3: $H_2CO$ absorption lines between 6547 $cm^{-1}$ and 6804 $cm^{-1}$ with absorption cross-sections, $\sigma$, greater than $0.5 \times 10^{-21}$ $cm^2$.

| $\tilde{\nu}$ | $\sigma$ | $\tilde{\nu}$ | $\sigma$ | $\tilde{\nu}$ | $\sigma$ |
|---|---|---|---|---|---|
| [$cm^{-1}$] | [$10^{-21}$ $cm^2$] | [$cm^{-1}$] | [$10^{-21}$ $cm^2$] | [$cm^{-1}$] | [$10^{-21}$ $cm^2$] |
| 6567.402 | 0.71 | 6652.368 | 0.70 | 6739.425 | 1.04 |
| 6567.418 | 0.60 | 6653.443 | 1.07 | 6741.337 | 1.08 |
| 6576.402 | 0.59 | 6654.459 | 0.76 | 6741.819 | 1.00 |
| 6576.425 | 0.77 | 6654.802 | 0.55 | 6743.692 | 1.26 |
| 6592.086 | 0.57 | 6654.868 | 0.57 | 6744.231 | 1.22 |
| 6595.268 | 0.63 | 6655.834 | 1.11 | 6746.066 | 0.99 |
| 6596.641 | 0.53 | 6656.654 | 0.83 | 6746.640 | 1.38 |
| 6596.731 | 0.53 | 6657.316 | 0.64 | 6748.460 | 1.16 |
| 6598.324 | 0.85 | 6657.355 | 0.62 | 6749.057 | 1.09 |
| 6598.359 | 1.00 | 6658.252 | 0.84 | 6750.868 | 1.32 |
| 6600.261 | 0.97 | 6658.718 | 0.69 | 6751.471 | 1.14 |
| 6601.348 | 0.89 | 6659.809 | 0.69 | 6753.294 | 1.19 |
| 6602.345 | 1.00 | 6659.828 | 0.69 | 6753.884 | 1.10 |
| 6604.211 | 1.18 | 6660.637 | 0.52 | 6754.619 | 0.56 |
| 6604.509 | 1.00 | 6660.711 | 0.89 | 6755.735 | 0.97 |
| 6606.318 | 0.54 | 6662.285 | 0.84 | 6756.286 | 0.95 |
| 6606.489 | 0.51 | 6663.242 | 0.74 | 6758.194 | 0.79 |
| 6606.723 | 1.13 | 6664.739 | 1.10 | 6758.682 | 1.19 |

– continued from previous page

| $\tilde{\nu}$ [cm$^{-1}$] | $\sigma$ [$10^{-21}$ cm$^2$] | $\tilde{\nu}$ [cm$^{-1}$] | $\sigma$ [$10^{-21}$ cm$^2$] | $\tilde{\nu}$ [cm$^{-1}$] | $\sigma$ [$10^{-21}$ cm$^2$] |
|---|---|---|---|---|---|
| 6606.964 | 1.12 | 6667.186 | 0.95 | 6760.665 | 0.54 |
| 6607.740 | 0.61 | 6667.433 | 0.53 | 6761.070 | 0.56 |
| 6608.975 | 1.10 | 6669.390 | 0.55 | 6763.774 | 0.53 |
| 6609.622 | 1.35 | 6669.625 | 0.67 | 6766.298 | 0.64 |
| 6610.538 | 0.55 | 6670.321 | 0.51 | 6767.336 | 0.69 |
| 6611.256 | 1.39 | 6672.197 | 0.52 | 6775.121 | 0.59 |
| 6612.212 | 1.40 | 6681.776 | 1.67 | 6775.757 | 0.67 |
| 6613.559 | 0.83 | 6684.691 | 0.54 | 6777.411 | 0.87 |
| 6614.757 | 1.18 | 6685.278 | 0.53 | 6778.311 | 0.83 |
| 6615.879 | 1.06 | 6686.209 | 0.54 | 6779.693 | 1.04 |
| 6617.276 | 1.13 | 6693.920 | 0.77 | 6780.872 | 1.01 |
| 6618.209 | 1.06 | 6695.400 | 0.93 | 6781.956 | 1.29 |
| 6619.780 | 0.92 | 6696.342 | 0.74 | 6782.003 | 0.73 |
| 6620.550 | 0.89 | 6696.805 | 0.51 | 6783.441 | 0.97 |
| 6622.281 | 0.77 | 6697.739 | 0.58 | 6784.213 | 1.24 |
| 6622.896 | 0.76 | 6698.758 | 1.02 | 6786.020 | 1.09 |
| 6624.779 | 0.93 | 6701.165 | 1.15 | 6786.457 | 1.15 |
| 6625.248 | 0.53 | 6703.558 | 0.85 | 6788.603 | 1.37 |
| 6638.777 | 0.51 | 6705.933 | 0.59 | 6788.699 | 1.24 |
| 6638.804 | 0.52 | 6705.953 | 0.59 | 6790.930 | 0.91 |
| 6639.331 | 0.61 | 6708.654 | 0.55 | 6791.191 | 1.27 |
| 6639.845 | 0.62 | 6709.633 | 0.68 | 6793.169 | 1.23 |
| 6641.674 | 0.78 | 6710.621 | 0.51 | 6793.778 | 1.25 |
| 6642.355 | 0.72 | 6710.678 | 0.65 | 6795.409 | 1.32 |
| 6644.015 | 0.66 | 6712.921 | 0.53 | 6795.959 | 0.97 |
| 6644.854 | 0.91 | 6717.946 | 0.56 | 6796.368 | 1.23 |
| 6646.361 | 0.92 | 6727.917 | 0.55 | 6797.668 | 1.09 |
| 6647.331 | 0.83 | 6729.629 | 0.65 | 6798.804 | 0.54 |
| 6648.712 | 1.13 | 6730.104 | 0.80 | 6798.952 | 1.12 |
| 6649.264 | 0.51 | 6732.042 | 0.97 | 6799.771 | 0.67 |
| 6649.675 | 0.58 | 6732.369 | 0.82 | 6799.955 | 1.08 |
| 6649.769 | 0.94 | 6734.362 | 1.05 | 6801.522 | 0.83 |
| 6649.839 | 0.58 | 6734.689 | 1.06 | 6802.281 | 1.19 |
| 6651.069 | 0.94 | 6736.676 | 1.11 | 6803.447 | 0.53 |
| 6652.157 | 0.96 | 6737.044 | 0.99 | 6804.058 | 0.87 |
| 6652.260 | 0.63 | 6738.999 | 1.23 | 6804.362 | 0.57 |

The complete absorption spectrum of $H_2CO$ from 6547 to 6804 cm$^{-1}$ is shown in Fig. 5. The multiple transitions and overlapping rovibrational combination bands produce a congested spectrum, making it difficult to assign individual absorption lines. The rotational envelopes of the fundamental modes are

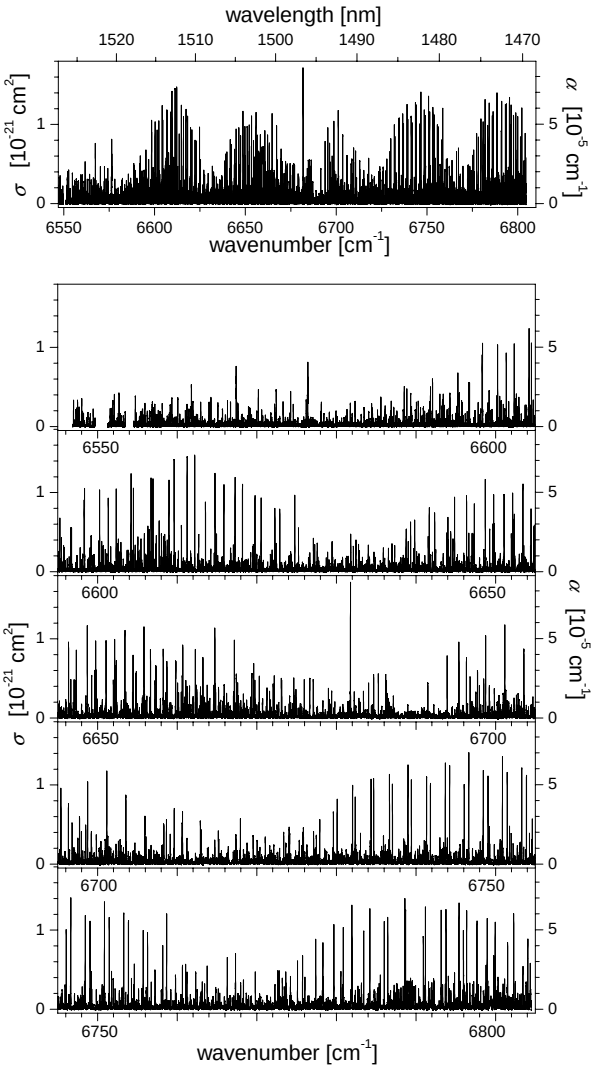


Fig. 5. The absorption spectrum of $H_2CO$ from 6550 to 6800 $cm^{-1}$. The top panel shows the complete spectrum; the spectrum is broken into 50 $cm^{-1}$ sections in the lower panels.

slightly greater than 100 $cm^{-1}$ wide at room temperature [22]; the width should be similar for the combination bands. Apparent rovibrational bands occur from 6590 to 6680 $cm^{-1}$, from 6720 to above 6800 $cm^{-1}$, and possibly from 6650 to 6730 $cm^{-1}$. These lines correspond most closely to the $3_1 4_2 5_1$ (6636 $cm^{-1}$), $2_1 3_1 4_3$ (6693 $cm^{-1}$), and $2_1 3_1 4_2 6_1$ (6778 $cm^{-1}$) combination bands reported by Bouwens et al. (also see Table 2). However, a comprehensive spectral analysis will be necessary to deconvolute the overlapping combination bands and to assign the vibrational frequencies with precision. Such an analysis is beyond the scope of this study. The strongest absorption lines in the spectrum (those with absorption cross-sections greater than $5 \times 10^{-22}$ $cm^2$) are listed in Table 3. This cut-off criterion results in 162 lines; the entire spectrum, in which over 8000 lines have been identified, is available in the supplementary

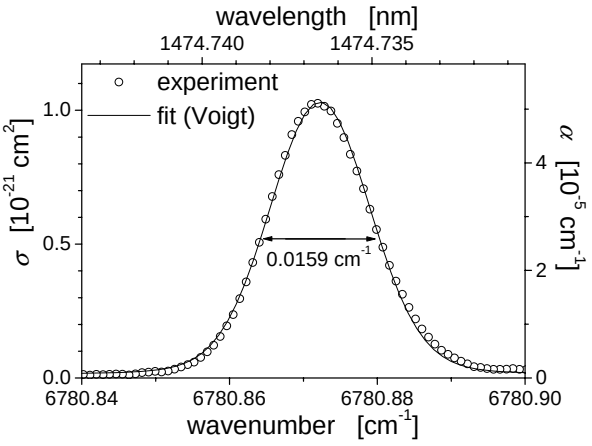


Fig. 6. Fit of a Voigt profile to the 6780 $cm^{-1}$ absorption line of pure $H_2CO$ at 2 mbar. Fit parameters for Voigt: Gaussian FWHM=0.00151 $cm^{-1}$, Lorentzian FWHM=0.00015 $cm^{-1}$. Empirical FWHM=0.0159 $cm^{-1}$.

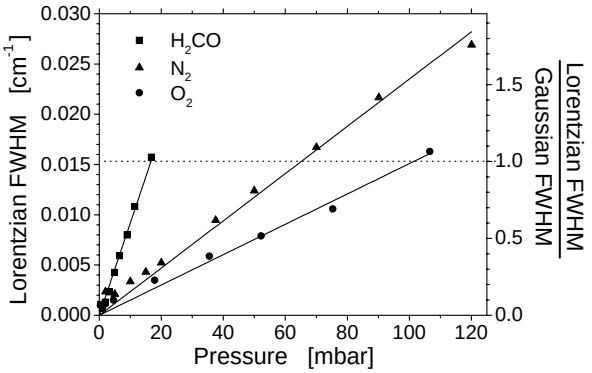


Fig. 7. Broadening of the 6780.871 $cm^{-1}$ line in $N_2$, $O_2$, and $H_2CO$, showing the Lorentzian FHWM (left axis) and the ratio of Lorentzian to Gaussian FWHM (right axis).

material [21]. The integrated absorption cross-section of the 6780.871 $cm^{-1}$ transition is $1.6 \times 10^{-23}$ cm/molecule and that of the 6684.053 $cm^{-1}$ transition is $7.2 \times 10^{-24}$ cm/molecule. The former transition is about 35 times weaker than the 5676.21 $cm^{-1}$ transition of the $2\nu_5$ overtone, and over 4000 times weaker than the $\nu_1$ C–H stretch [2].

### *3.2 Pressure broadening*

The pressure broadening of the 6780.871 $cm^{-1}$ line in $N_2$, $O_2$, and $H_2CO$, and of the 6684.053 $cm^{-1}$ line in $N_2$, was studied. For different pressures of pure $H_2CO$, Voigt profiles were fitted to the absorption lines using a non-linear least square method (Levenberg-Marquardt) [23]. From the Voigt fits the Lorentzian and Gaussian contributions to the overall FWHM were de-

Table 4
Pressure broadening of $H_2CO$ absorption lines at ≈291 K for the transitions at 6780.871 $cm^{-1}$ and 6684.053 $cm^{-1}$. The Gaussian contribution to the FWHM of 0.015 $cm^{-1}$ (determined at 2 mbar $H_2CO$) was fixed for each gas investigated.

| Transition [$cm^{-1}$] | Gas | FWHM pressure broadening [$10^{-4} cm^{-1} mbar^{-1}$] |
|---|---|---|
| 6780.871 | $H_2CO$ | 9.18 ± 0.18 |
| 6780.871 | $O_2$ | 1.51 ± 0.05 |
| 6780.871 | $N_2$ | 2.35 ± 0.05 |
| 6684.058 | $N_2$ | 2.01 ± 0.10 |

termined. The measurements showed that at pressures ≤2 mbar the FWHM was entirely dominated by Doppler broadening. The corresponding value of 0.0151 $cm^{-1}$ for the Gaussian width agreed with the laboratory temperature within the uncertainty of the Voigt fit ($8 \times 10^{-4}$ $cm^{-1}$). A Voigt fit to the experimental data for $H_2CO$ at 2 mbar is shown in Fig. 6. The quality of this fit was slightly affected by an adjacent absorption line; however, the resulting additional uncertainty of the FWHM was negligible. For each series of pressure dependent measurements in $N_2$ and $O_2$ the first measurement was performed with pure $H_2CO$ before adding the respective buffer gas. The Gaussian FWHM (0.015 $cm^{-1}$) was then fixed in Voigt fits of absorption measurements in $N_2$ and $O_2$ at higher pressures. The Lorentzian pressure broadening contribution to the FWHM increases linearly with pressure for all the gases, as shown in Fig. 7 for the line at 6780.871 $cm^{-1}$. The effect of the $H_2CO$ pressure is much more marked than that of $N_2$ and $O_2$. Table 4 lists the corresponding broadening parameters, which were obtained by linear regression of the Lorentzian widths versus pressure. The broadening parameters determined in $N_2$ for the two different absorption lines agree reasonably well. The small discrepancy can result from the fact that the 6780.871 $cm^{-1}$ line is well isolated, whereas the line at 6684.058 $cm^{-1}$ may have an underlying additional absorption feature, which can be attributed to the small asymmetry of the line. The errors stated in the table only refer to the quality of the linear fit. Finally, no pressure shift in the peak positions was observed within our experimental uncertainty.

## 4 Summary

We have measured the formaldehyde spectrum from 6547 to 6804 $cm^{-1}$ (1527 to 1470 nm) with a resolution of about 0.001 $cm^{-1}$ using CEAS. The absorption cross-section for the spectrum was estimated by comparison to the known

linestrengths of $CO_2$ and $H_2O$. The pressure broadening coefficients in $N_2$ have been determined for two absorption lines.

## Acknowledgements

We are grateful to Professor M.W.D. Mansfield (Physics Dept., UCC) and Professor P. Brint (Chemistry Dept., UCC) for their continued support and interest in our work. We would like to thank Dr. A. Allanic (Centre for Research into Atmospheric Chemistry, UCC) for his assistance in sample preparation, as well as J. Lucey, J. Sheehan, and D. Kearney (UCC) for their technical assistance. This work received funding by the HEA ($2^{nd}$ cycle, AC3 Environ. Chem.) and IRCSET (SC/2002/160), whose support we gratefully acknowledge.

## References

[1] R.P. Wayne, Chemistry of Atmospheres, Oxford University Press, Oxford, 2000.

[2] H.R. Barry, L. Corner, G. Hancock, R. Peverall, G.A.D. Ritchie, Phys. Chem. Chem. Phys. 4 (2002) 445–450.

[3] A. Fried, B.P. Wert, B. Henry, J.R. Drummond, Spectrochim. Acta A 55 (1999) 2097–2110.

[4] J.D. DeSain, A.D. Ho, C.A. Taatjes, J. Mol. Spectrosc. 219 (2003) 163–169.

[5] S. Pinceloup, G. Laverdet, F. Maguin, J.F. Doussin, P. Carlier, G. Le Bras, J. Photochem. Photobiol. A 157 (2003) 275–281.

[6] C.A. Taatjes, D.B. Oh, Appl. Opt. 36 (1997) 5817–5821.

[7] T.J. Johnson, F.G. Wienhold, J.P. Burrows, G.W. Harris, J. Phys. Chem. 95 (1991) 6499–6502.

[8] H. Dahnke, G. von Basum, K. Kleinermanns, P. Hering, M. Murtz, Appl. Phys. B 75 (2002) 311–316.

[9] A. O'Keefe, D.A.G. Deacon, Rev. Sci. Instrum. 59 (1988) 2544–2551.

[10] R. Engeln, G. Berden, R. Peeters, G. Meijer, Rev. Sci. Instrum. 69 (1998) 3763–3769.

[11] L. Corner, H.R. Barry, G. Hancock, Chem. Phys. Lett. 374 (2003) 28–32.

[12] N.M. Poulin, M.J. Bramley, T. Carrington Jr., H.G. Kjaergaard, B.R. Henry, J. Chem. Phys. 104 (1996) 7807–7820.

[13] R.J. Bouwens, J.A. Hammerschmidt, M.M. Grzeskowiak, T.A. Stegink, P.M. Yorba, W.F. Polik, J. Chem. Phys. 104 (1996) 460–479.

[14] A. O'Keefe, J.J. Scherer, J.B. Paul, Chem. Phys. Lett. 307 (1999) 343–349.

[15] S.E. Fiedler, A. Hese, A.A. Ruth, Chem. Phys. Lett. 371 (2003) 284–294.

[16] S.E. Fiedler, A. Hese, A.A. Ruth, Rev. Sci. Instrum. to be submitted (2004).

[17] J.B. Paul, L. Lapson, J.G. Anderson, Appl. Opt. 40 (2001) 4904–4910.

[18] L. Lundsberg-Nielsen, F. Hegelund, F.M. Nicolaisen, J. Mol. Spectrosc. 162 (1993) 230–245.

[19] No $NH_3$ lines were observed in two scans covering the region from 6629.1 to 6632.8 $cm^{-1}$. To calibrate the wavenumber scale in this region, the positions of adjacent, overlapping formaldehyde lines were used to fix the wavenumber values at one end of the spectrum. The relative wavenumber markers from the etalon were used as described in the text. We estimate a wavenumber uncertainty of 0.003 $cm^{-1}$ in this region.

[20] L.S. Rothman, R.R. Gamache, A. Goldman, L.R. Brown, R.A. Toth, H.M. Pickett, R.L. Poynter, J.-M. Flaud, C. Camy-Peyret, A. Barbe, N. Husson, C.P. Rinsland, M.A.H. Smith, Appl. Opt. 26 (1987) 4058–4097.

[21] The entire spectrum and a list of spectral regions containing less reliable data are available at *http://www.sciencedirect.com* or *http://msa.lib.ohio–state.edu/jmsa_hp.htm*.

[22] G. Herzberg, Molecular Spectra and Molecular Structure: Vol. II. Infrared and Raman Spectra of Polyatomic Molecules, Van Nostrand, Princeton, 1968.

[23] M. Woydyr, *http://fityk.sf.net*, woydyr@if.pw.edu.pl.

**Table**

Table 1
Transition energies for the six normal vibrational modes of $H_2CO$ [12].

| Number | Symmetry | $\tilde{\nu}$ [$cm^{-1}$] | Mode |
|---|---|---|---|
| $\nu_1$ | $a_1$ | 2782.5 | $CH_2$ symmetric stretch |
| $\nu_2$ | $a_1$ | 1746.0 | CO stretch |
| $\nu_3$ | $a_1$ | 1500.2 | $CH_2$ scissor |
| $\nu_4$ | $b_1$ | 1167.3 | $CH_2$ wag |
| $\nu_5$ | $b_2$ | 2843.3 | $CH_2$ asymmetric stretch |
| $\nu_6$ | $b_2$ | 1249.1 | $CH_2$ rock |

**Table**

Table 2
Combination bands between 6500 and 6830 $cm^{-1}$ from the dispersed fluorescence spectra of Bouwens et al. [13]. Tentatively identified combination bands observed in our spectrum are indicated with asterisks.

| Combination band | Symmetry | $\tilde{\nu}$ [$cm^{-1}$] |
|---|---|---|
| $3_2 4_2 6_1$ | $b_2$ | 6508.8 |
| $1_1 3_1 4_2$ | $a_1$ | 6562.7 |
| $2_1 4_2 6_2$ | $a_1$ | 6578.8 |
| $1_2 4_1$ | $b_1$ | 6611.6 |
| $3_1 4_2 5_1$ | $b_2$ | 6635.7* |
| $2_3 3_1$ | $a_1$ | 6652.2 |
| $2_1 3_1 4_3$ | $b_1$ | 6693.4* |
| $3_1 4_1 5_1 6_1$ | $b_1$ | 6710.0 |
| $3_1 5_1 6_2$ | $b_2$ | 6759.0 |
| $2_1 3_1 4_2 6_1$ | $b_2$ | 6777.6* |
| $4_1 5_2$ | $b_1$ | 6795.1 |
| $3_3 4_2$ | $a_1$ | 6815.2 |
| $1_1 2_1 4_2$ | $b_1$ | 6825.5 |

**Table**

Table 3: $H_2CO$ absorption lines between 6547 $cm^{-1}$ and 6804 $cm^{-1}$ with absorption cross-sections, $\sigma$, greater than $0.5 \times 10^{-21}$ $cm^2$.

| $\tilde{\nu}$ [$cm^{-1}$] | $\sigma$ [$10^{-21}$ $cm^2$] | $\tilde{\nu}$ [$cm^{-1}$] | $\sigma$ [$10^{-21}$ $cm^2$] | $\tilde{\nu}$ [$cm^{-1}$] | $\sigma$ [$10^{-21}$ $cm^2$] |
|---|---|---|---|---|---|
| 6567.402 | 0.71 | 6652.368 | 0.70 | 6739.425 | 1.04 |
| 6567.418 | 0.60 | 6653.443 | 1.07 | 6741.337 | 1.08 |
| 6576.402 | 0.59 | 6654.459 | 0.76 | 6741.819 | 1.00 |
| 6576.425 | 0.77 | 6654.802 | 0.55 | 6743.692 | 1.26 |
| 6592.086 | 0.57 | 6654.868 | 0.57 | 6744.231 | 1.22 |
| 6595.268 | 0.63 | 6655.834 | 1.11 | 6746.066 | 0.99 |
| 6596.641 | 0.53 | 6656.654 | 0.83 | 6746.640 | 1.38 |
| 6596.731 | 0.53 | 6657.316 | 0.64 | 6748.460 | 1.16 |
| 6598.324 | 0.85 | 6657.355 | 0.62 | 6749.057 | 1.09 |
| 6598.359 | 1.00 | 6658.252 | 0.84 | 6750.868 | 1.32 |
| 6600.261 | 0.97 | 6658.718 | 0.69 | 6751.471 | 1.14 |
| 6601.348 | 0.89 | 6659.809 | 0.69 | 6753.294 | 1.19 |
| 6602.345 | 1.00 | 6659.828 | 0.69 | 6753.884 | 1.10 |
| 6604.211 | 1.18 | 6660.637 | 0.52 | 6754.619 | 0.56 |
| 6604.509 | 1.00 | 6660.711 | 0.89 | 6755.735 | 0.97 |
| 6606.318 | 0.54 | 6662.285 | 0.84 | 6756.286 | 0.95 |
| 6606.489 | 0.51 | 6663.242 | 0.74 | 6758.194 | 0.79 |
| 6606.723 | 1.13 | 6664.739 | 1.10 | 6758.682 | 1.19 |
| 6606.964 | 1.12 | 6667.186 | 0.95 | 6760.665 | 0.54 |
| 6607.740 | 0.61 | 6667.433 | 0.53 | 6761.070 | 0.56 |
| 6608.975 | 1.10 | 6669.390 | 0.55 | 6763.774 | 0.53 |
| 6609.622 | 1.35 | 6669.625 | 0.67 | 6766.298 | 0.64 |
| 6610.538 | 0.55 | 6670.321 | 0.51 | 6767.336 | 0.69 |
| 6611.256 | 1.39 | 6672.197 | 0.52 | 6775.121 | 0.59 |
| 6612.212 | 1.40 | 6681.776 | 1.67 | 6775.757 | 0.67 |
| 6613.559 | 0.83 | 6684.691 | 0.54 | 6777.411 | 0.87 |
| 6614.757 | 1.18 | 6685.278 | 0.53 | 6778.311 | 0.83 |
| 6615.879 | 1.06 | 6686.209 | 0.54 | 6779.693 | 1.04 |
| 6617.276 | 1.13 | 6693.920 | 0.77 | 6780.872 | 1.01 |
| 6618.209 | 1.06 | 6695.400 | 0.93 | 6781.956 | 1.29 |
| 6619.780 | 0.92 | 6696.342 | 0.74 | 6782.003 | 0.73 |
| 6620.550 | 0.89 | 6696.805 | 0.51 | 6783.441 | 0.97 |
| 6622.281 | 0.77 | 6697.739 | 0.58 | 6784.213 | 1.24 |
| 6622.896 | 0.76 | 6698.758 | 1.02 | 6786.020 | 1.09 |
| 6624.779 | 0.93 | 6701.165 | 1.15 | 6786.457 | 1.15 |
| 6625.248 | 0.53 | 6703.558 | 0.85 | 6788.603 | 1.37 |
| 6638.777 | 0.51 | 6705.933 | 0.59 | 6788.699 | 1.24 |
| 6638.804 | 0.52 | 6705.953 | 0.59 | 6790.930 | 0.91 |
| 6639.331 | 0.61 | 6708.654 | 0.55 | 6791.191 | 1.27 |
| 6639.845 | 0.62 | 6709.633 | 0.68 | 6793.169 | 1.23 |
| 6641.674 | 0.78 | 6710.621 | 0.51 | 6793.778 | 1.25 |

– continued from previous page

| $\tilde{\nu}$ [cm$^{-1}$] | $\sigma$ [$10^{-21}$ cm$^2$] | $\tilde{\nu}$ [cm$^{-1}$] | $\sigma$ [$10^{-21}$ cm$^2$] | $\tilde{\nu}$ [cm$^{-1}$] | $\sigma$ [$10^{-21}$ cm$^2$] |
|---|---|---|---|---|---|
| 6642.355 | 0.72 | 6710.678 | 0.65 | 6795.409 | 1.32 |
| 6644.015 | 0.66 | 6712.921 | 0.53 | 6795.959 | 0.97 |
| 6644.854 | 0.91 | 6717.946 | 0.56 | 6796.368 | 1.23 |
| 6646.361 | 0.92 | 6727.917 | 0.55 | 6797.668 | 1.09 |
| 6647.331 | 0.83 | 6729.629 | 0.65 | 6798.804 | 0.54 |
| 6648.712 | 1.13 | 6730.104 | 0.80 | 6798.952 | 1.12 |
| 6649.264 | 0.51 | 6732.042 | 0.97 | 6799.771 | 0.67 |
| 6649.675 | 0.58 | 6732.369 | 0.82 | 6799.955 | 1.08 |
| 6649.769 | 0.94 | 6734.362 | 1.05 | 6801.522 | 0.83 |
| 6649.839 | 0.58 | 6734.689 | 1.06 | 6802.281 | 1.19 |
| 6651.069 | 0.94 | 6736.676 | 1.11 | 6803.447 | 0.53 |
| 6652.157 | 0.96 | 6737.044 | 0.99 | 6804.058 | 0.87 |
| 6652.260 | 0.63 | 6738.999 | 1.23 | 6804.362 | 0.57 |

**Table**

Table 4
Pressure broadening of $H_2CO$ absorption lines at ≈291 K for the transitions at 6780.871 $cm^{-1}$ and 6684.053 $cm^{-1}$. The Gaussian contribution to the FWHM of 0.015 $cm^{-1}$ (determined at 2 mbar $H_2CO$) was fixed for each gas investigated.

| Transition [$cm^{-1}$] | Gas | FWHM pressure broadening [$10^{-4} cm^{-1} mbar^{-1}$] |
|---|---|---|
| 6780.871 | $H_2CO$ | 9.18 ± 0.18 |
| 6780.871 | $O_2$ | 1.51 ± 0.05 |
| 6780.871 | $N_2$ | 2.35 ± 0.05 |
| 6684.058 | $N_2$ | 2.01 ± 0.10 |

Figure

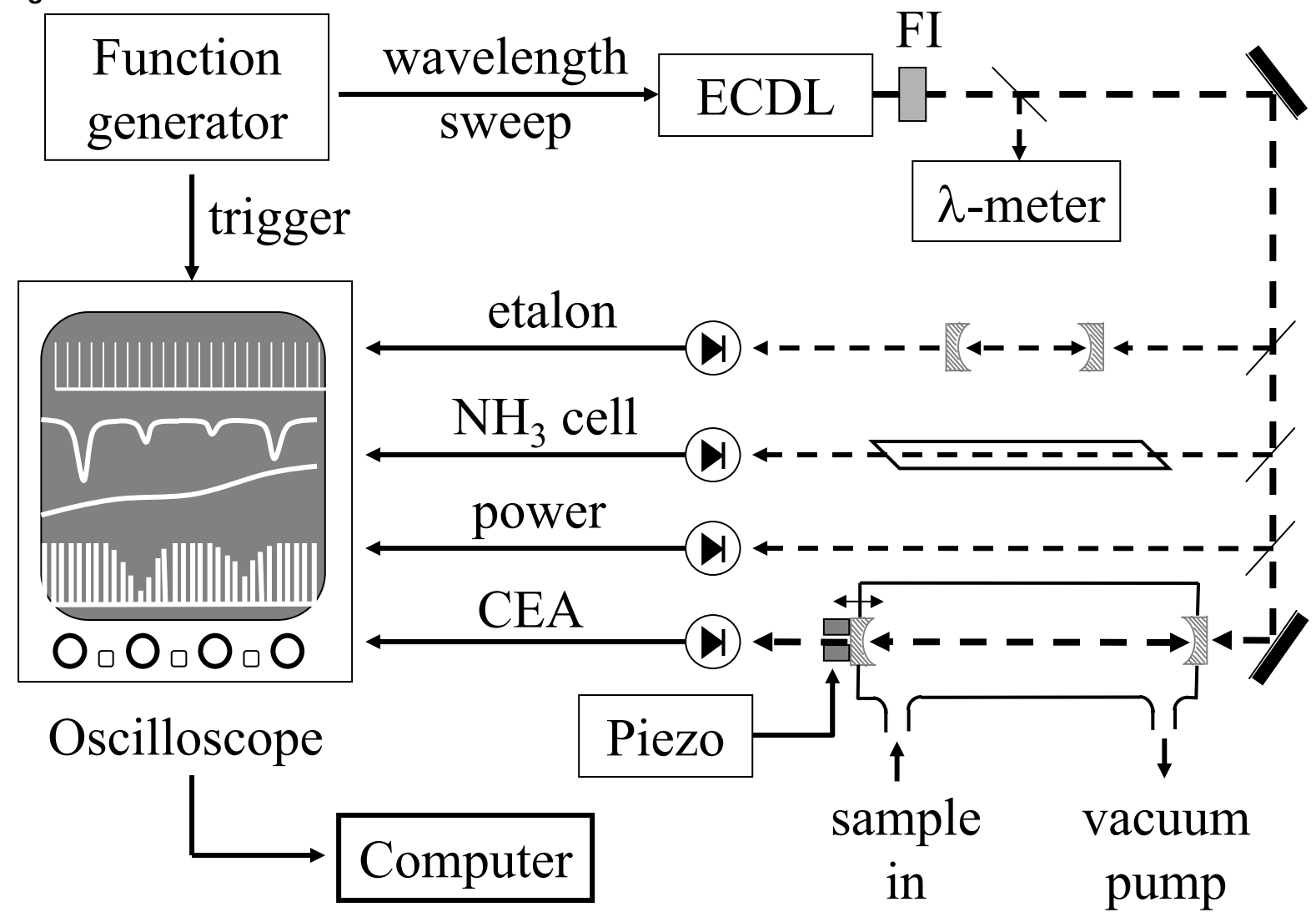
Function generator
wavelength sweep
ECDL
FI
λ-meter
trigger
etalon
NH3 cell
power
CEA
Piezo
Oscilloscope
Computer
sample in
vacuum pump

**Figure**

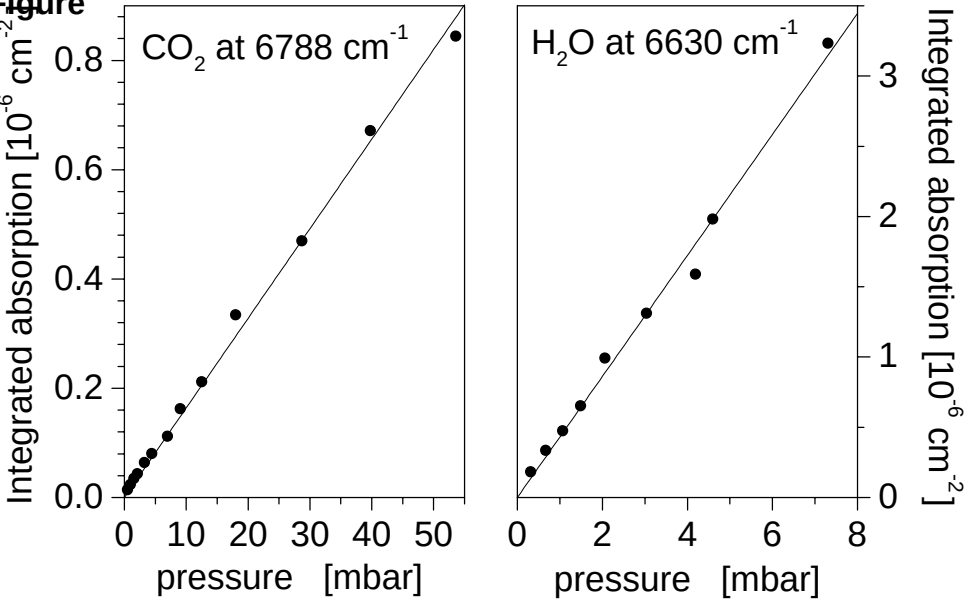
CO2 at 6788 cm-1
H2O at 6630 cm-1
Integrated absorption [10-6 cm-2]
pressure [mbar]
pressure [mbar]
0.0
0.2
0.4
0.6
0.8
0
10
20
30
40
50
0
2
4
6
8
0
1
2
3

**Figure**

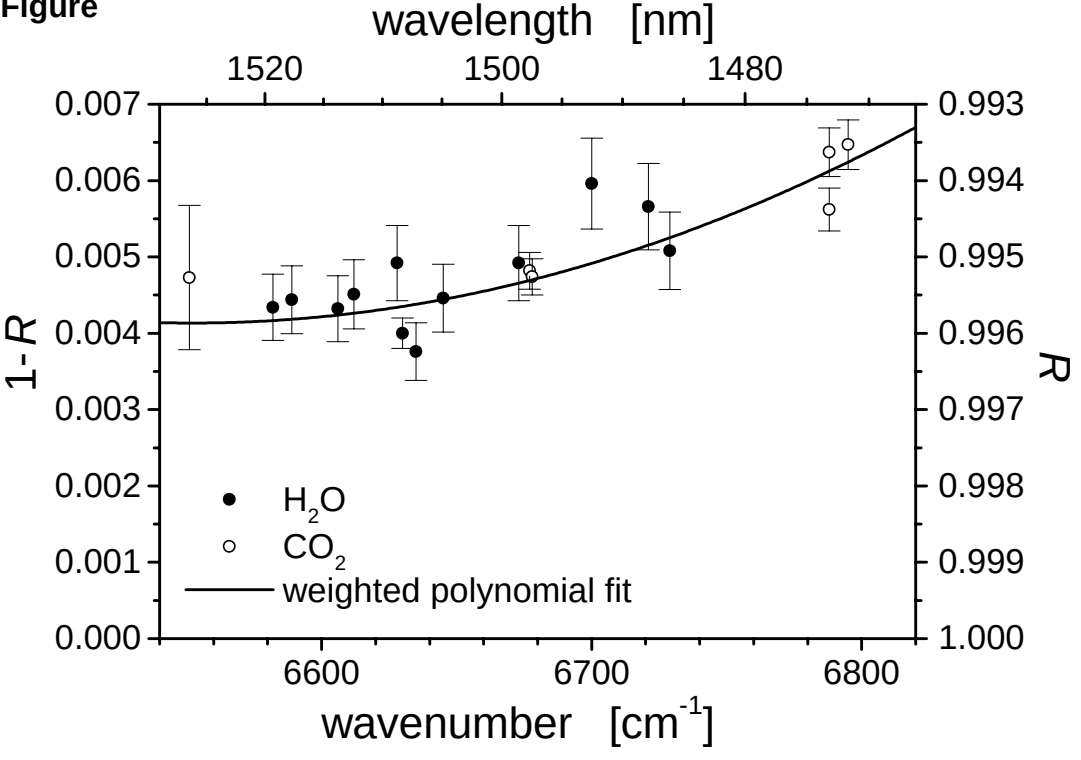
wavelength [nm]
1520
1500
1480
0.007
0.006
0.005
0.004
0.003
0.002
0.001
0.000
1-R
0.993
0.994
0.995
0.996
0.997
0.998
0.999
1.000
R
H2O
CO2
weighted polynomial fit
6600
6700
6800
wavenumber [cm-1]

**Figure**

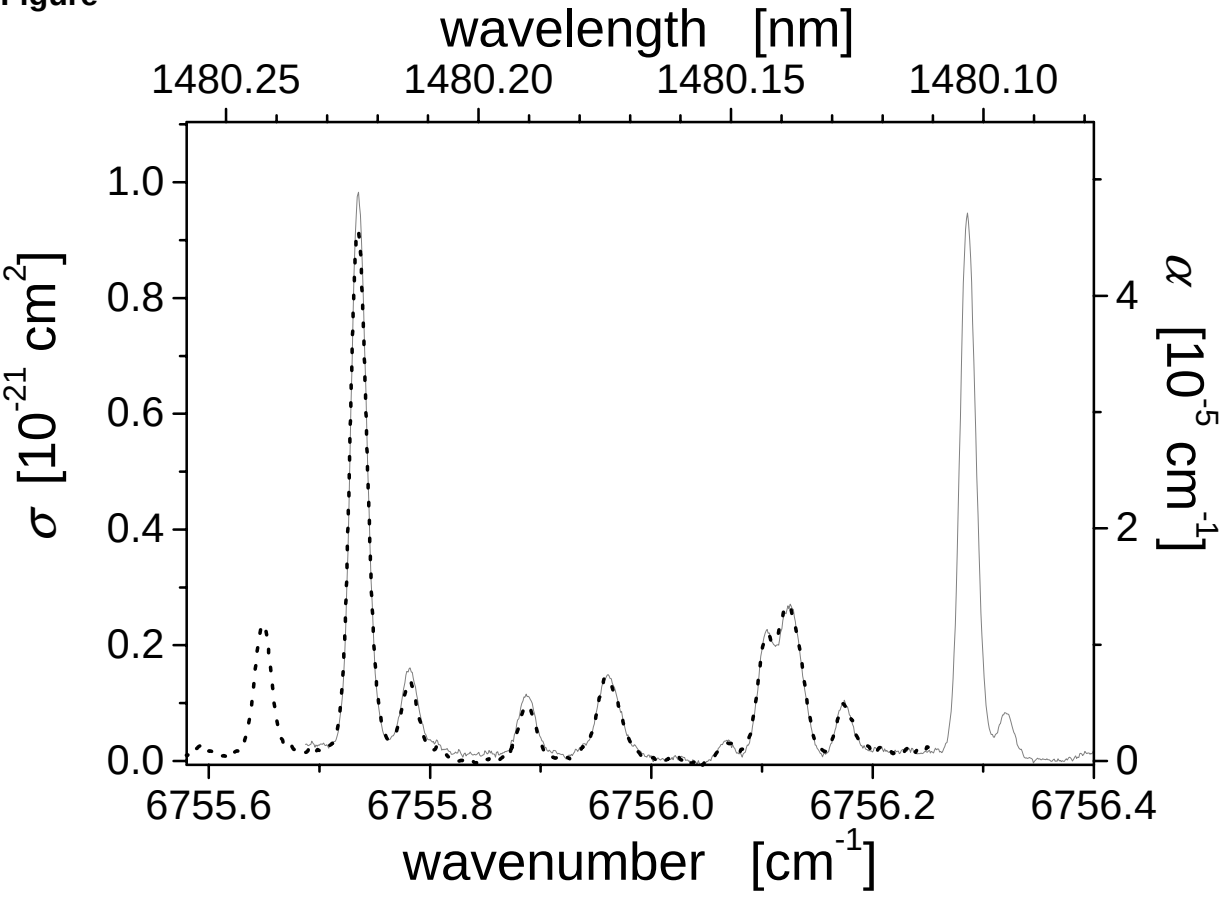
wavelength [nm]
1480.25
1480.20
1480.15
1480.10
σ [10^-21 cm^2]
α [10^-5 cm^-1]
1.0
0.8
0.6
0.4
0.2
0.0
4
2
0
6755.6
6755.8
6756.0
6756.2
6756.4
wavenumber [cm^-1]

**Figure**

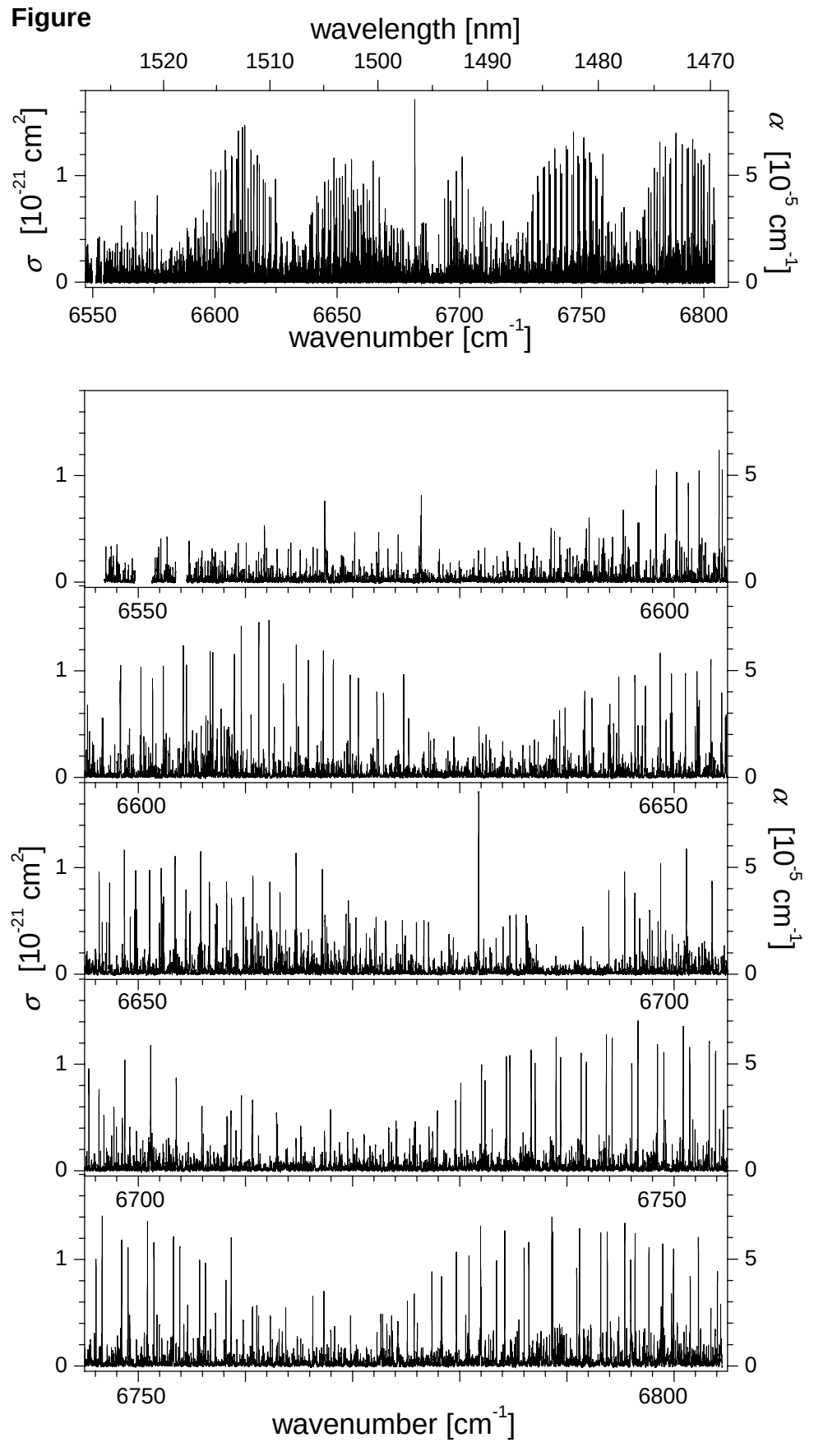
wavelength [nm]
1520
1510
1500
1490
1480
1470
σ [10^-21 cm^2]
α [10^-5 cm^-1]
6550
6600
6650
6700
6750
6800
wavenumber [cm^-1]

**Figure**

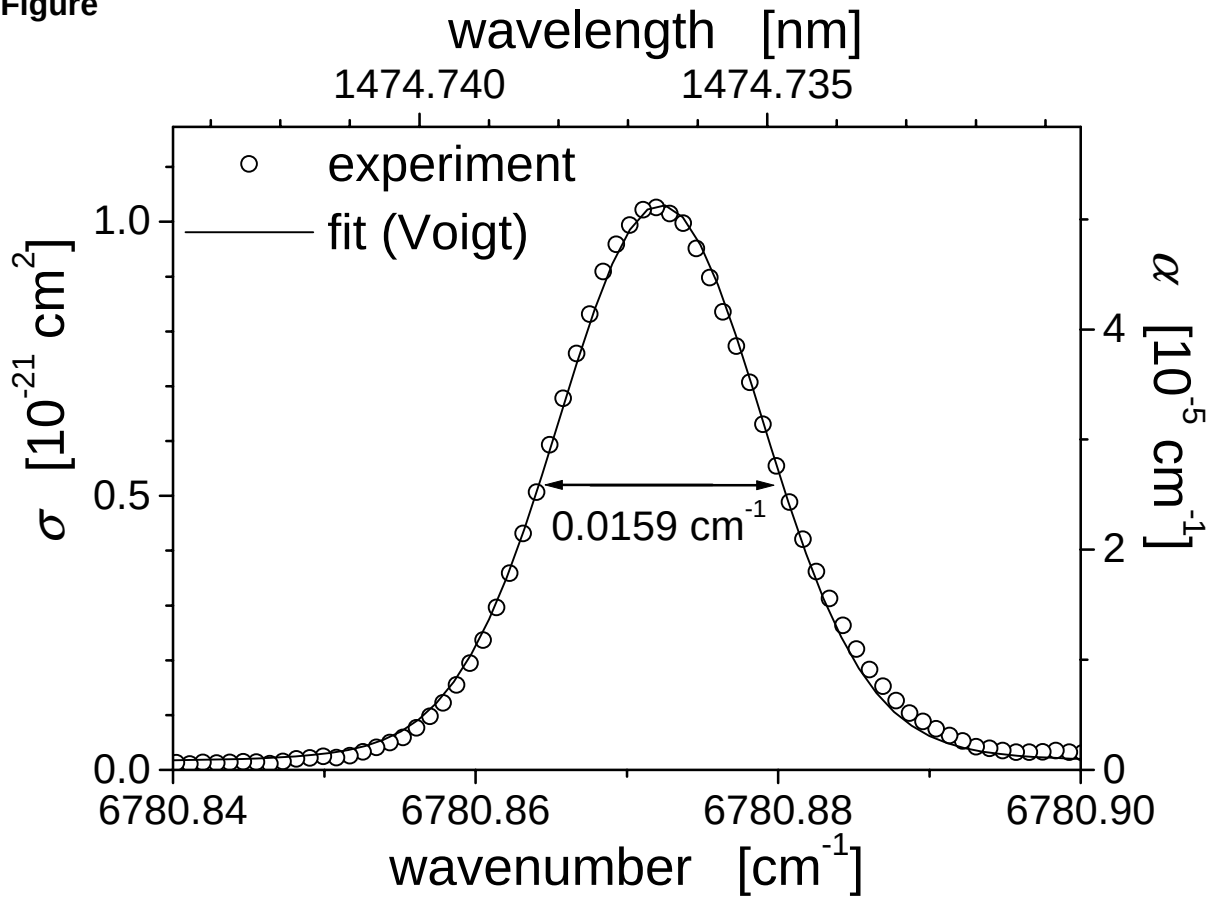
wavelength [nm]
1474.740
1474.735
experiment
fit (Voigt)
1.0
0.5
0.0
σ [10^-21 cm^2]
α [10^-5 cm^-1]
4
2
0
0.0159 cm^-1
6780.84
6780.86
6780.88
6780.90
wavenumber [cm^-1]

**Figure**

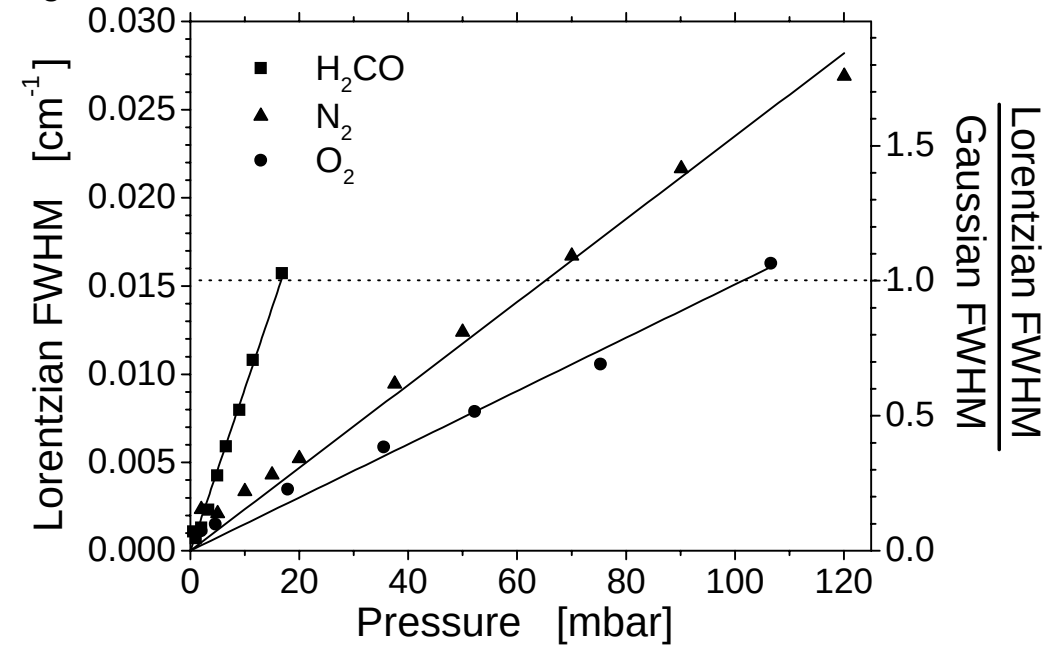
0.030
0.025
0.020
0.015
0.010
0.005
0.000
Lorentzian FWHM [cm-1]
H2CO
N2
O2
0
20
40
60
80
100
120
Pressure [mbar]
1.5
1.0
0.5
0.0
Lorentzian FWHM
Gaussian FWHM

# Explan.txt File (for Supplementary Material)

The supplementary material for the web
consists of two additional files - the second file could not be
uploaded on submission.

(A) Supplementary text: Staak_et_al_Supplement1.doc (Word file)
Outlines regions (3%) of the published spectrum where errors
are somewhat larger than the general uncertainties stated in
the main manuscript. Reference is made in the main text - Ref. [21].

(B) Original data of measured spectrum:
We intended to provide the full spectrum, comprising over 8000
absorption features, as supplementary material, since it is
of interest for database development and atmospheric modelling.
However, the online submission system does not allow the uploading
of ordinary ASCII data or zipped files.
The original ASCII data file has a size of 6.4 MB.
The zipped data (using WinZip) has a size of 1.9 MB.
If the data were embedded in a WORD document it would be
27 MB which is unacceptable.

Eventually we would like to provide the spectrum on the web in
zipped ASCII form, if that is possible - please advice how to
proceed with the submission of these data. E-mail: a.ruth@ucc.ie

# The rotationally-resolved absorption spectrum of formaldehyde from 6547 to 6804 $cm^{-1}$

***– Supplementary Material –***

M. Staak, E.W. Gash, D.S. Venables, A.A. Ruth*

*Department of Physics, National University of Ireland, University College Cork, Cork, Ireland*

Submitted to the Journal of Molecular Spectroscopy, 7 July 2004.

## Absorption spectrum

The full spectrum is available as supplementary material in two data columns;
1st column: $\tilde{\nu}$ [$cm^{-1}$], 2nd column: $\sigma$ [$10^{-21}$ $cm^2$ / molecule].

## Less accurate spectral regions

Based on the accuray of the mirror reflectivity as a function of wavelength, a maximum systematic uncertainty of the absorption cross-section of ±5% was established. An additional statistical uncertainty of less than 10% was established for the general measurement error of the absorption – both estimates are conservative.

Less than 3% of the overall spectrum have a larger statistical uncertainty of 25% in the absorption due to an insufficient overlap or inadequate correspondency of spectral segments to satisfactorily verify the absorption in these regions.

| Spectral region [$cm^{-1}$] |
|---|
| 6546.86 – 6547.20 |
| 6549.40 – 6549.70 |
| 6551.26 – 6551.92 |
| 6553.20 – 6553.51 |
| 6558.10 – 6559.00 |
| 6559.30 – 6559.80 |
| 6564.80 – 6565.10 |
| 6575.60 – 6575.20 |
| 6598.00 – 6598.30 |
| 6612.15 – 6612.25 |
| 6613.50 – 6614.80 |
| 6643.60 – 6644.00 |
| 6655.20 – 6655.60 |

6662.80 – 6663.00
6726.70 – 6727.10
6733.80 – 6734.20
6798.40 – 6799.50

In the spectral regions listed below a shift in the wavenumber position was observed for the same absorption lines in different overlapping spectral segments. The shifts may be due to (a) unnoticed mode-hops of the laser or (b) discrepancies in the calibration data of $NH_3$ absorption lines. The region and the wavenumber difference between the corresponding lines is reported.

| Spectral region [$cm^{-1}$] | Wavenumber shift [$cm^{-1}$] |
|---|---|
| 6673.90 – 6674.74 | 0.005 |
| 6677.70 – 6678.20 | 0.004 |
| 6695.35 – 6695.45 | 0.004 |
| 6782.90 – 6782.10 | 0.007 |
| 6753.40 – 6754.10 | 0.007 |
| 6783.00 – 6783.60 | 0.005 |
| 6794.30 – 6794.50 | 0.005 |
| 6630.75 – 6630.85 | 0.003 |
| 6681.75 – 6681.85 | 0.004 |
| 6800.65 – 6801.20 | 0.010 |

We regard the following spectral region as rather uncertain in both wavenumber and absorption cross-section:

| Spectral region [$cm^{-1}$] |
|---|
| 6801.20 – 6802.16 |